



Water-soluble iron emitted from vehicle exhaust is linked to primary speciated organic compounds

Joseph R. Salazar¹, Benton T. Cartledge¹, John P. Haynes¹, Rachel York-Marini¹, Allen L. Robinson², Greg T. Drozd⁴, Allen H. Goldstein³, Sirine C. Fakra⁵, and Brian J. Majestic¹

¹University of Denver, Department of Chemistry and Biochemistry, Denver, CO, USA

²Carnegie Mellon University, College of Engineering, Pittsburgh, PA, USA

³University of California, Berkeley Department of Civil and Environmental Engineering, Berkeley, CA, USA

⁴Colby College, Department of Chemistry, Waterville, ME, USA

⁵Advanced Light Source, Lawrence Berkeley National Laboratory, Berkeley, CA 94720, USA

Correspondence: Brian J. Majestic (brian.majestic@du.edu)

Received: 23 April 2019 – Discussion started: 19 September 2019

Revised: 14 December 2019 – Accepted: 15 January 2020 – Published: 17 February 2020

Abstract. Iron is the most abundant transition element in airborne particulate matter (PM), primarily existing as Fe(II) or Fe(III). Generally, the fraction of water-soluble iron is greater in urban areas compared to areas dominated by crustal emissions. To better understand the origin of water-soluble iron in urban areas, tailpipe emission samples were collected from 32 vehicles with emission certifications of Tier 0 low emission vehicles (LEV I), Tier 2 low emission vehicles (LEV II), ultralow emission vehicles (ULEVs), super-ultralow emission vehicles (SULEVs), and partial-zero emission vehicles (PZEVs). The components quantified included gases, inorganic ions, elemental carbon (EC), organic carbon (OC), total metals, and water-soluble metals. Naphthalene and intermediate-volatility organic compounds (IVOCs) were quantified for a subset of vehicles. The IVOCs quantified contained 12 to 18 carbons and were divided into three subgroups: aliphatic, single-ring aromatic (SRA), and polar (material not classified as either aliphatic or SRA). Iron solubility in the tested vehicles ranged from 0% to 82% (average 30%). X-ray absorption near-edge structure (XANES) spectroscopy showed that Fe(III) was the primary oxidation state in 14 of the 16 tested vehicles, confirming that the presence of Fe(II) was not the main driver of water-soluble Fe. The correlation of water-soluble iron with sulfate was insignificant, as was correlation with every chemical component except naphthalene and some C12–C18 IVOCs with R^2 values as high as 0.56. A controlled benchtop study confirmed that naphthalene alone increases iron solubility from

soils by a factor of 5.5 and that oxidized naphthalene species are created in the extract solution. These results suggest that the large driver in water-soluble iron from primary vehicle tailpipe emissions is related to the organic composition of the PM. We hypothesize that, during the extraction process, specific components of the organic fraction of the PM are oxidized and chelate the iron into water.

1 Introduction

Iron has been identified as a limiting nutrient for phytoplankton in approximately half of the world's oceans, with deposition from the atmosphere as the major source (Moore and Abbott, 2002; Sholkovitz et al., 2012). Phytoplankton is one of the controlling factors of fixed nitrogen in many parts of the oceans and consequently plays a major role in the ocean's biogeochemical cycles (Baker et al., 2006; Chen and Siefert, 2004; Kraemer, 2004; Shi et al., 2012; Tagliabue et al., 2017). Also, water-soluble iron fractions are linked to the creation of reactive oxygen species (ROSs) in lung fluid and in environmental matrices through Fenton chemistry (Hamad et al., 2016). These ROSs impart oxidative stress on the respiratory system, contributing to various health effects (Landreman et al., 2008; Park et al., 2006; Verma et al., 2014).

Annually, approximately 55 Tg of iron enters the atmosphere from crustal sources (Luo et al., 2008). Of this, 14–16 Tg is deposited into the ocean, impacting the marine life

and influencing the ecosystems (Gao, 2003; Jickells et al., 2005). Typically, airborne iron from crustal sources ranges from 0.05 % to 2 % water-soluble iron of the total iron (Bonnet, 2004; Sholkovitz et al., 2012). Relative water-soluble iron in urban environments is higher, ranging from 2 % to 50 % of the total (Majestic et al., 2007; Sedwick et al., 2007; Sholkovitz et al., 2012). It is suggested that combustion sources including fossil fuel burning, incinerator use, and biomass burning may be a large contributor to the water-soluble iron fraction, contributing $0.66\text{--}1.07\text{ Tg a}^{-1}$ of water-soluble iron, and this iron has been correlated with anthropogenic sources (Chuang et al., 2005; Luo et al., 2008; Sholkovitz et al., 2009). From these combustion sources, it has been shown that the species of iron differed greatly and had an impact on iron solubility (Fu et al., 2012). Even though total iron emissions from combustion sources are small in comparison to crustal sources, the relative insolubility of crustal iron leads to the possibility that combustion sources contribute 20 %–100 % of water-soluble iron into the atmosphere (Luo et al., 2008; Sholkovitz et al., 2012).

Previous studies in tunnels and parking structures have reported iron ranging from 5 to approximately 3500 ng m^{-3} , revealing that brake wear, tire wear, resuspended road dust, and tailpipe emissions can be important sources of trace elements (Kuang et al., 2017; Lawrence et al., 2013; Li and Xiang, 2013; Lough et al., 2005; Park et al., 2006; Verma et al., 2014). Iron is contained in many fuels with precombusted concentrations ranging from 13 to $1000\text{ }\mu\text{g L}^{-1}$ (Lee and Von Lehmden, 1973; Santos et al., 2011; Teixeira et al., 2007). Computational models of combustion in engines suggest that iron emissions could also originate from the fuel injector nozzle inside the engine block (Liati et al., 2015).

There are many different factors that may contribute to water-soluble iron, and as a result several different hypotheses have been developed relating to how iron is solubilized in ambient atmospheres. First, the correlation of ambient iron with sulfates in ambient aerosols suggests the possibility of iron solubilization (Desboeufs et al., 1999; Hand et al., 2004; Mackie et al., 2005; Oakes et al., 2012b). However, laboratory studies investigating the heterogeneous chemistry of iron have not shown any change in iron water solubility, speciation, or oxidation state upon exposure to gaseous SO_2 (Cartledge et al., 2015; Luo et al., 2005; Majestic et al., 2007; Oakes et al., 2012a). A second hypothesis is that the particle-bound iron oxidation state may control iron water solubility. Thus far, the limited field studies have been unable to show that the iron oxidation state is correlated with iron's resulting water solubility, as the majority of iron found in aerosol particles is in the less soluble Fe(III) oxidation state (Luo et al., 2005; Majestic et al., 2007; Oakes et al., 2012a). A third, broad, iron solubilization hypothesis emphasizes an iron–organic interaction (Baba et al., 2015; Vile et al., 1987). For example, a significant increase in water-soluble iron is observed in the presence of oxalate and formate in ambient aerosols and in cloud droplets (Paris et al., 2011; Zhu et al.,

1993). Even when compared to sulfuric acid, oxalic acid results in a greater increase in iron solubility because of the organic iron interaction (Chen and Grassian, 2013). Other studies have suggested that the photolysis of polycyclic aromatic hydrocarbons leads to reduced iron, which may result in greater iron water solubility (Faiola et al., 2011; Haynes and Majestic, 2019; Haynes et al., 2019; Pehkonen et al., 1993; Zhu et al., 1993). Vehicle exhaust contains many organic species, including secondary organic aerosol (SOA), single-ring aromatic compounds (C6–C9), polycyclic aromatic hydrocarbons (PAHs), hopanes, steranes, alkanes, organic acids, and intermediate-volatility organic compound (IVOCs), which are longer-chain organic species (Cheung et al., 2010; Zhao et al., 2016).

In this study, we explore all three hypotheses (bulk ions, iron oxidation state, and organic speciation) in relation to iron solubility. Specifically, we examine the water-soluble iron emitted from 32 light-duty gasoline vehicles with certifications of Tier 0 low emission vehicles (LEV I), Tier 2 low emission vehicles (LEV II), ultralow emission vehicles (ULEVs), super-ultralow emission vehicles (SULEVs), and partial-zero emission vehicles (PZEVs). The total and water-soluble trace elements are compared to the ions, gaseous compounds, and organic emissions from the same vehicle set. Additionally, we acquired data on the emitted iron oxidation states on the exhaust particles. From this data set, real tailpipe emission samples were explored to discover how various components of automobile exhaust affect the water solubility of iron.

2 Materials and methods

2.1 Sample collection

Exhaust samples from 32 gasoline vehicles were collected at the California Air Resources Board (CARB) Haagen–Smit laboratory over a 6-week period. Standard emission test results from this campaign have been reported previously (Saliba et al., 2017). A description of the dynamometer, emission dilution system, and instrumentation used in the vehicle setup is provided elsewhere (May et al., 2014; Saliba et al., 2017). Briefly, each vehicle was tested on a dynamometer using the cold-start Unified California (UC) Drive Cycle or the hot-start Modal Arterial Cycle 4. Emission samples were collected using a constant volume sampler (CVS) from which a slipstream of dilute exhaust was drawn at a flow rate of 47 L min^{-1} . Particle-phase emissions were collected using three sampling trains operated in parallel off the end of the CVS dilution tunnel. Train 1 contained a Teflon filter (47 mm, Pall-Gelman, Teflo R2PJ047). Train 2 contained two quartz filters (47 mm, Pall-Gelman, Tissuquartz 2500 QA0UP) in series. Train 3 contained an acid-cleaned Teflon filter followed by a quartz filter (47 mm, Teflo, Pall Life Sciences, Ann Arbor, MI), and the flow rate was 0.5 L min^{-1}

through each Tenax tube. The particulate exhaust emissions were then collected on the pre-cleaned Teflon filters. The Teflon filters were stored in a freezer until extraction and analysis was performed. Filter holders were maintained at 47 °C during sampling as per the CFR86 protocol.

The vehicles were recruited from private citizens, rental car agencies, or part of the Air Resource Board fleet. The vehicles tested were categorized by model years (1990–2014), vehicle type (passengers car and light-duty trucks), engine technologies (GDI and PFI), emission certification standards (Tier 1 to SULEVs), make, and model. All vehicles were tested using the same commercial gasoline fuel, which had a 10 % ethanol blend and a carbon fraction of 0.82 (Saliba et al., 2017).

Gases (CO, CO₂, CH₄, NO, and NO₂) and total hydrocarbons (THCs) were collected into heated Tedlar bags by UC Drive Cycles. Analysis of CO and CO₂ was conducted by nondispersive infrared detectors (IRD-4000), CH₄ by gas chromatography with detection by a flame ionization detector (FID), NO_x by chemiluminescence (CLD 4000), and THC by FID (Drozd et al., 2016; Saliba et al., 2017). The Teflon filter in Train 1 was analyzed by ion chromatography for water-soluble anions and cations, and the procedure for these data is presented elsewhere (Hickox et al., 2000). Train 2 included two parallel sets of Tenax-TA sorbent tubes (Gerstel) downstream of the Teflon filter. The first set was two tubes connected in parallel. One of these tubes was used to collect emissions during the cold-start phase of UC (the first 5 min, commonly referred to as bag 1). The other tube was used to sample emissions during the combined hot-running and hot-start phases of the UC (bags 1 and 2). The second set of sorbent tubes was connected in series to collect emissions over the entire UC test. The Teflon filter in Train 3 was used for total and water-soluble trace element analysis and particle-bound iron oxidation state; it is the focus of this study.

2.2 Material preparation

All vessel cleaning and analytical preparation for the trace elements was performed under a laminar flow hood with incoming air passing through a high-efficiency particulate air (HEPA) filter. All water used was purified to 18.2 MΩ cm (Milli-Q Thermo-Fisher Nanopore); 15 mL and 50 mL plastic centrifuge vials, Petri dishes (Fisher), Teflon forceps (Fisher), syringes (Fisher), nitro cellulose paper (Fisher), and syringe cases (Life Sciences Products) were prepped by an acid-cleaning process. For the plastic centrifuge vials, Petri dishes, Teflon forceps, syringe, and syringe cases this involved 24 h soaks in a 10 % reagent-grade nitric acid bath, followed by a 10 % reagent-grade hydrochloric bath, then a 3 % trace-metal-grade nitric acid (Fisher) resting bath with MQ rinses before, after, and between each step. The nitro cellulose paper was cleaned by soaking in 2 % HCl for 24 h then rinsing with MQ water. Then, 2 % HCl and MQ water were

pushed through the filter. Teflon beaker liners were cleaned by an acetone rinse, then an overnight bath of 100 % HPLC-grade (high-performance liquid chromatography) acetonitrile and a final overnight bath of 5 % trace-metal-grade nitric acid. The 0.20 micron syringe filters (Whatman, Marlborough, MA) were prepared with 10 % trace-metal-grade hydrochloric acid, MQ water, and a 5 % nitric acid rinse.

The 47 mm Teflon filters were cleaned by submerging them in 10 % trace-metal-grade nitric acid and rinsing with MQ water. The filters were then stored in the acid-cleaned Petri dishes and sealed with Teflon tape for storage.

2.3 Water-soluble metal sample preparations

Water-soluble elements were extracted for 2 h from the Teflon filter on a shaker table in 10 mL of MQ water. The water extract was filtered with 2 μm pore size nitro cellulose filters. The Teflon filter and the nitro cellulose filters were saved for total metal digestion. The water-soluble element extract was acidified to 5 % trace-metal-grade nitric acid and 2.5 % trace-metal-grade hydrochloric acid to be analyzed by inductively coupled plasma mass spectrometry (ICP-MS; Agilent 7700).

2.4 Sample preparation for total elemental analysis

First, ~ 3 % (measured exactly) of the filters were cut and saved for X-ray absorption near-edge structure (XANES) spectroscopy; then the water-soluble elements were extracted, and the polymethylpentene ring was removed from the Teflon filters. The Teflon and the nitro cellulose filters for each sample were placed together into a microwave digestion vessel. To each digestion vessel, 750 μL of concentrated trace-metal-grade nitric acid, 250 μL of concentrated trace-grade hydrochloric acid, 100 μL of concentrated trace-grade hydrofluoric acid, and 100 μL of 30 % hydrogen peroxide were added. These samples were digested (Ethos EZ, Milestone Inc) according to the following temperature program: 15 min ramp to 200 °C, then held at 200 °C for 15 min, and a 60 min cooling period (Cartledge and Majestic, 2015). The samples were cooled to room temperature for 1 h, and the solution was diluted to 15 mL with MQ water and analyzed via ICP-MS.

2.5 Elemental analysis

Blank filters and standard reference materials (SRMs) were digested alongside the exhaust samples using the same digestion process described above. Three SRMs were used to address the recoveries of our digestion process: urban particulate matter (1648a, NIST), San Joaquin soil (2709a, NIST), and recycled auto-catalyst (2556, NIST). The recoveries of the SRMs were between 80 % and 120 %. The elements analyzed included Na, Mg, Al, K, Ca, Ti, V, Cr, Mn, Fe, Co, Ni, Cu, Zn, As, Se, Rb, Sr, Mo, Rh, Pd, Ag, Cd, Sb, Cs, Ba, Ce, Pt, Pb, and U. Indium (~ 1 ppb) was used as an internal

standard, and a He collision cell was used to remove isobaric interferences.

2.6 XANES spectroscopy

X-ray absorption near-edge structure (XANES) and micro X-ray fluorescence (μ XRF) data for 16 vehicle exhaust samples were collected at the Advanced Light Source Microprobe beamline (10.3.2), Lawrence Berkeley National Laboratory, Berkeley, CA (Marcus et al., 2004). To locate iron spots on the filters, a broad μ XRF elemental map of each sample was acquired at 10 keV using 12 μ m by 12 μ m pixel size and 50 ms of dwell time per pixel. The μ XRF spectra were simultaneously recorded on each pixel of the map. Iron oxidation state and iron-bearing phases were investigated using iron K-edge extended XANES. The spectra were recorded in fluorescence mode by continuously scanning the Si (111) monochromator (Quick XAS mode) from 7011 to 7415 eV. The data were calibrated using an iron foil with the first derivative set at 7110.75 eV (Kraft et al., 1996). All data were recorded using a seven-element solid-state Ge detector (Canberra, ON). The spectra were dead-time corrected, deglitched, calibrated, pre-edge background subtracted, and post-edge normalized using a suite of LabVIEW custom programs available at the beamline (Marcus et al., 2008). To rapidly survey the iron oxidation state, a valence scatter plot was generated from normalized XANES data using a custom MATLAB code and a large database of iron standards (10.3.2 XAS database) (Marcus et al., 2008). Least-squares linear combination fitting (LCF) was subsequently performed in the range 7090 to 7365 eV to confirm iron valence and further identify the major mineral groups present. The best fit was chosen based on (1) the minimum normalized sum-square value ($NSS = 100 \times [\sum(\mu_{\text{exp}} - \mu_{\text{fit}})^2 / \sum(\mu_{\text{exp}})^2]$), for which the addition of a spectral component to the fit required a 10 % or greater improvement in the NSS value, and (2) on the elements detected in the μ XRF spectrum recorded on each XANES spot. The uncertainty on the percentages of species present is estimated to be ± 10 %.

2.7 Organic speciation

A subset of 10 of the 32 samples was quantified for IVOCs using electron impact ionization with methods similar to that of Zhao et al., except adapted for GCxGC methods (Zhao et al., 2015, 2016). IVOC material was classified into three categories: aliphatic, single-ring aromatic (SRA), and polar (Drozd et al., 2019). Classification within these three classes of compounds was determined by differences in second-dimension retention time (polarity space) and by mass spectral characteristics in our GCxGC–MS analysis. All three classes of compounds were quantified by either compound-specific calibration using known standards or relating total ion chromatogram (TIC) signals to calibration standards of similar volatility and polarity. In GCxGC, the TIC signal

corresponds to a blob, or a region in volatility and polarity retention space. The GC-Image software package was used to create blobs from 2-D chromatograms. Compounds were quantified by relating their TIC signal to that of the nearest standard in terms of polarity and volatility. Volatility bins were defined that are evenly spaced with their center elution times corresponding to each *n*-alkane. TIC blobs were quantified using the calibration for the available standard of similar polarity in the same volatility bin.

2.8 Emission factor calculations

Emissions data are presented as fuel-based emission factors (EFs). Emission factors are calculated as the amount of analyte emitted by mass per gram of fuel emitted.

$$EF_i (\text{kg fuel}^{-1}) = \Delta m_i \frac{x_c(g)}{\Delta \text{CO}_2(g) + \Delta \text{CO}(g) + \Delta \text{THC}(g)} \quad (1)$$

ΔCO_2 , ΔCO , and ΔTHC are the background-corrected carbon concentration of CO_2 , CO, and THC (Drozd et al., 2016; Goldstein et al., 2017), respectively. x_c is the fuel carbon mass fraction of 0.82. Δm_i is the blank-subtracted concentrations of species *i*.

2.9 Naphthalene and iron benchtop study

To better understand the production of soluble iron during the water extraction process, a benchtop study was performed using three varying forms of iron with naphthalene. The iron stock solutions and suspensions included (1) standardized San Joaquin soil (NIST SRM 2709a) containing 25 ppm total iron (soluble + insoluble) to determine the effects of crustal iron, (2) iron(II) sulfate to a concentration of 25 ppm to examine the effect of a soluble iron(II) source, and (3) iron(III) sulfate to examine a source of soluble iron(III). In parallel, 100 mg of naphthalene crystals was added to 200 mL of MQ water. For the experiment, 99 mL of the naphthalene suspension and 1 mL of the iron suspension were added to Teflon liners (250 ppb iron total), which were inserted into a jacketed glass beaker temperature controlled to 25 °C. After 16 h of stirring, 2 mL was filtered (0.2 μ m) and acidified to 5 % nitric acid. Soluble iron released from the soil in both the presence and absence of naphthalene was analyzed by ICP-MS. Chemical changes in naphthalene in the presence and absence of iron were monitored by HPLC.

3 Results and discussion

3.1 Total and water-soluble element exhaust concentrations

Emissions of ions, organic species, gaseous species, and EC/OC from these tests have been published previously (Drozd et al., 2016, 2019; Goldstein et al., 2017; Saliba et al., 2017). In order to obtain a better understanding of the factors

that influence iron solubility, we compare these with the total elements, trace elements, and iron oxidation state measurements. Generally, the elements with the highest EF are the lighter crustal elements Ca, Al, and Fe, with average EF of 200, 100, and 80 μg per kg fuel (Table 1), respectively. Iron has the third-highest average EF of all the elements and the highest of all transition elements, ranging from 0 to 200 μg Fe per kg fuel. This is followed by three first-row transition elements: Zn, Cu, and Ni, with the respective average EF of 60, 20, and 5 μg per kg fuel. Other notable elements include Rh, Pd, and Pt, likely originating from the catalytic converter, with the respective average EF of 0.05, 0.7, and 0.04 μg per kg fuel. Toxic elements include chromium, lead, molybdenum, and antimony with respective EF of 5, 0.8, 5, and 0.2 μg per kg fuel. A previous study has shown that various elements are enriched in used motor oil, such as copper, zinc, manganese, iron, and lead, which could originate from engine wear (Majestic et al., 2009).

Table 1 also shows the EF for the water-soluble fraction of the trace elements. The water-soluble EF for iron ranges from 0 to 150 μg per kg fuel, or 0 % to 82 % of the total. At 20 μg per kg fuel, average water-soluble iron was the third-largest EF of all elements. There were relatively high emissions of a few other water-soluble elements such as Ca with an average EF of 200 μg per kg fuel and Zn with tailpipe emissions averaging 40 μg per kg fuel.

Only a few studies report tailpipe emissions (i.e., dynamometer testing) of trace elements for diesel- and gasoline-powered passenger cars, and even fewer have reported water-soluble iron. Table 2 compares the average exhaust particulate matter (PM) composition and trace elements in distance-based emission factors in this study to literature values for other passenger vehicles, including one diesel and three gasoline exhaust studies. For all elements, the distance-based emission factors were greater in the diesel cohort relative to the gasoline vehicles. Compared to previous studies, the trace elements emitted from older gasoline passenger vehicles resulted in an order of magnitude higher emissions for all elements, except for aluminum, which only showed a factor of ~ 2 increase in older vehicles (Table 2). Iron shows a large range in the three studies of gasoline vehicles, ranging from 8.3 to 280 $\mu\text{g km}^{-1}$ compared to the 0–62 $\mu\text{g km}^{-1}$ measured in this study.

The large ranges in iron solubility from previous studies led us to explore and compare the newer emission certification standard (Figs. 1 and 2). Total iron did not trend strongly with the emission certification standard, although on average total iron is less in the Tier 0 vehicles and LEVs. Water-soluble iron shows a small average decrease of approximately 5 μg per kg fuel between ULEVs and SULEVs, with a further average decrease for the PZEVs of 3.9 μg per kg fuel.

Table 1. Average of total trace total and water-soluble elements from car exhaust reported in EF (μg per kg fuel). These samples represent a range of different makes and models of cars. The values in parentheses are the range of the vehicle population ($n = 32$).

	Total elements	Water-soluble elements
Trace elements (μg per kg fuel)		
Na	50 (0, 200)	30 (0, 100)
Mg	40 (0, 200)	8 (0, 60)
Al	100 (0, 2000)	20 (0, 100)
K	20 (0, 100)	20 (0, 100)
Ca	200 (0, 1000)	200 (0, 1000)
Ti	1 (0, 60)	0.2 (0, 2)
V	0.02 (0, 0.7)	0.02 (0, 0.7)
Cr	5 (0.04, 20)	0.6 (0, 4)
Mn	2 (0.02, 10)	1 (0.007, 8)
Fe	80 (0, 400)	20 (0, 200)
Co	0.2 (0, 1)	0.04 (0, 0.7)
Ni	5 (0, 30)	2 (0, 10)
Cu	20 (0, 200)	20 (0, 100)
Zn	60 (0, 300)	40 (0, 300)
As	0.006 (0, 0.03)	0.006 (0, 0.03)
Se	0.3 (0, 2)	0.05 (0, 0.5)
Rb	0.2 (0, 0.5)	0.01 (0, 0.1)
Sr	1 (0.01, 4)	0.6 (0.003, 3)
Mo	5 (0, 20)	3 (0.002, 30)
Rh	0.06 (0, 0.5)	0.007 (0, 0.1)
Pd	0.8 (0, 6)	0.3 (0, 4)
Ag	0.1 (0, 2)	0.03 (0, 0.5)
Cd	0.007 (0, 0.3)	0.009 (0, 0.05)
Sb	0.2 (0, 1)	0.1 (0, 0.9)
Cs	0.005 (0, 0.02)	0.002 (0, 0.02)
Ba	5 (0, 20)	3 (0.06, 20)
Ce	4 (0, 40)	0.4 (0, 2)
Pt	0.04 (0, 0.4)	0.01 (0, 0.2)
Pb	0.4 (0, 7)	0.3 (0, 7)
U	0.002 (0, 0.03)	0.002 (0, 0.03)

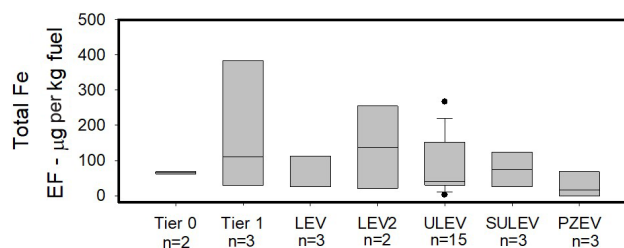


Figure 1. Total iron from the 32 vehicles tested reported in EF (μg per kg fuel). The center black line represents the median value and the edges of the boxes represent the 25th and 75th percentiles, while the whiskers extent are the 10th and 90th percentiles.

Table 2. Comparison of exhaust composition (g km^{-1}) from different dynamometer studies that included both gasoline- and diesel-powered light-duty vehicles. The values are the mean of the vehicle population, and the values in parentheses are the minimum and maximum values. This table is in grams per kilogram as opposed to grams per kilogram of fuel in Table 1.

	This study Gasoline ($n = 32$)	Gasoline (Schauer et al., 2002) ($n = 9$)	Gasoline (Norbeck et al., 1998) ($n = 40$)	Diesel (Norbeck et al., 1998) ($n = 19$)
Fleet age	1990–2014	1981–1994	1972–1990	1977–1993
PM components (mg km^{-1})				
OC	1 (0.06, 10)	3.3 ± 0.21	16 ± 32	150 ± 330
EC	10 (0.06, 100)	0.77 ± 0.023	3.5 ± 4.8	160 ± 100
Sulfate	0.02 (0.001, 0.1)	0.08 ± 0.16	0.93 ± 1.9	$0.77 \pm .93$
Trace elements ($\mu\text{g km}^{-1}$)				
Ag	0.01 (0, 0.25)	4.5 ± 20	0	0
Al	10 (0, 110)	20 ± 17	19 ± 37	31 ± 75
Ba	0.6 (0, 4.4)	0	0	68 ± 75
Ca	30 (0, 130)	26 ± 8.5	81 ± 120	650 ± 930
Cd	0.00 (0, 0.04)	0	0	0
Co	0.01 (0, 0.25)	–	0	0
Cr	0.6 (0.008, 4)	0	0	6.2 ± 12
Cu	3 (0, 27)	0	6.2 ± 6.2	19 ± 31
Fe	10 (0, 62)	8.3 ± 2.3	280 ± 680	830 ± 1000
K	2 (0, 15)	3.0 ± 11.3	0	50 ± 170
Mg	7 (0, 120)	–	25 ± 31	99 ± 200
Mn	0.2 (0.002, 1.3)	0	0	6.2 ± 6.2
Mo	0.5 (0, 3.6)	2.3 ± 6.8	0	6.2 ± 12
Ni	0.6 (0, 5.2)	0	6.2 ± 12	12 ± 18
Pb	0.04 (0, 0.57)	0	25 ± 93	19 ± 62
Sb	0.02 (0, 0.21)	17 ± 39	0	0
Sr	0.1 (0, 0.68)	0.75 ± 2.3	0	0
Zn	7 (0, 37)	14 ± 1.5	110 ± 170	810 ± 1500

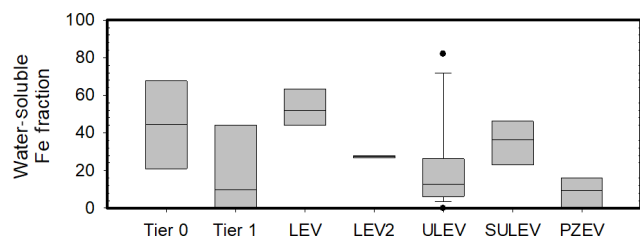


Figure 2. Water-soluble iron from the 32 vehicles tested reported in water-soluble iron fraction. The center black line represents the median value and the edges of the boxes represent the 25th and 75th percentiles, while the whiskers are the 10th and 90th percentiles.

3.2 Iron correlations with bulk exhaust components and iron oxidation state

To explore what factors and, if any, exhaust components are associated with the presence of water-soluble iron, linear regression analyses were used to compare soluble iron to different chemical species in the exhaust. Solubility from the

direct exhaust was explored by comparing the EFs of both sulfate and nitrate to iron, and water-soluble iron was not correlated with either of these species (Figs. 3 and S1 in the Supplement). The EFs for water-soluble iron and CO_2 showed no correlation, suggesting that overall fuel use was not an important factor for water-soluble iron production (Fig. S1). Total iron was correlated with the water-soluble iron, indicating that the total amount of iron may have an impact on soluble iron (Fig. S2). Finally, to evaluate if water-soluble iron and overall particulate carbon relate, the EFs for elemental carbon (EC) and organic carbon (OC) were compared to that of soluble iron, and again no correlation was observed (Figs. 3 and S1).

As no correlation between water-soluble iron and bulk chemical species was observed (Figs. S1 and S3), the importance of the particle-bound iron oxidation state was investigated. Since Fe(II) is known to be more soluble than Fe(III), the expectation was that exhaust samples having a large Fe(II) character would have a greater iron solubility relative to those containing Fe(III) or Fe(0) (Stumm and Morgan, 1996). Figure 3 presents a scatter plot of the iron

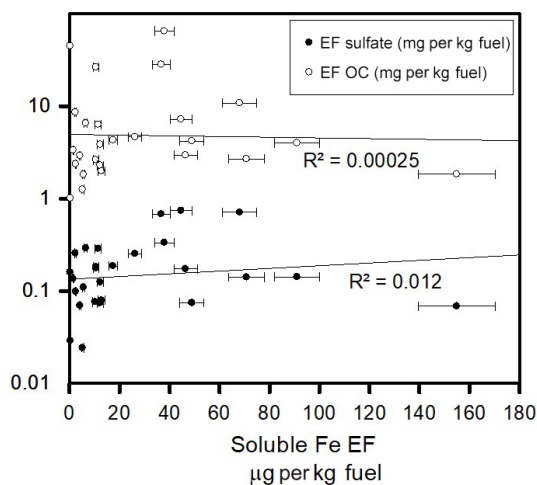


Figure 3. Linear correlation plots representing EF in milligrams per kilogram of fuel for sulfate and organic carbon (OC) in micrograms per kilogram of fuel for water-soluble iron. Correlation lines and R^2 values for all elements are shown.

valence in 16 of the exhaust samples compared with iron-bearing standards of known valence. This valence plot is generated from iron K-edge XANES data, wherein the parameters κ and μ are defined as normalized absorbance values at 7113 and 7117.5 eV, respectively. We observe that the exhaust iron is primarily in the Fe(III) oxidation state, except for two vehicles: sample 11, dominated by Fe(0), and sample 15, containing a combination of Fe(0) and Fe(III) (Fig. S4). Sample 11 is an extreme case, having 0% iron solubility and a highly elevated amount of EC at 305 $\mu\text{g per kg fuel}$ (study average 78 $\mu\text{g per kg fuel}$). The presence of Fe(0) is consistent with high EC, as both observations suggest a lack of oxidation during the combustion and emission process. While the valence plot (Fig. 3) put sample 15 as mostly Fe(II), the LCF actually showed that it was a mixture of Fe(0) and Fe(III). And this sample contained only 10% water-soluble iron, which is less than the cohort average. The study-wide solid-phase iron oxidation state is primarily Fe(III) or a mixed oxidation state (Fe(III) and Fe(0)) (see Fig. 3), averaging about 30% water-soluble iron, which is well above the crustal background.

LCF XANES fitting (Fig. S4) showed Fe(III) oxides and oxyhydroxides as the dominant group, followed by Fe(III) sulfates and iron silicates (Fig. S4). Hematite ($\alpha\text{-Fe}_2\text{O}_3$) and maghemite ($\gamma\text{-Fe}_2\text{O}_3$) were the most consistently detected Fe(III) oxides. Iron was detected in all samples, with Zn, Cr, and Cu as the main other elements detected in nearly all samples (detection of low- Z elements below sulfur or high- Z elements above zinc was not possible in our experimental conditions). Overall, these results strongly suggest that the main driver of water-soluble iron is not associated with the particle-bound iron oxidation state. Further investigation for the LCF XANES fitting showed that 34% of iron speciated

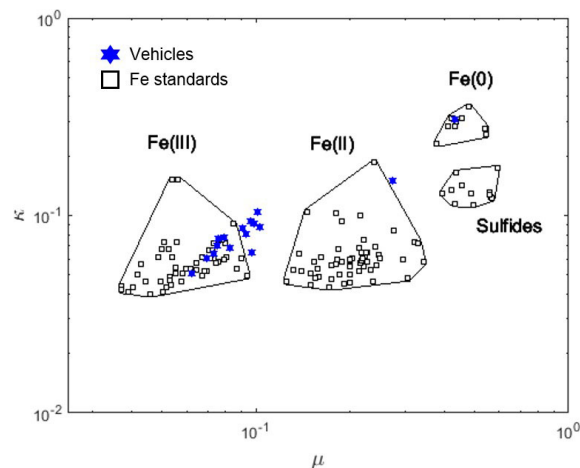


Figure 4. Fe valence scatter plot generated from Fe K-edge XANES data; κ and μ are normalized absorbance values at 7113 and 7117.5 eV, respectively. Empty black squares represent Fe standards of known valence, while blue-filled stars represent vehicle exhaust samples.

was Fe(III)-oxyhydroxides associated with organic material, leading to the investigation of organic species, which resulted in a correlation with longer-chain IVOCs and naphthalene (Fig. S6).

3.3 Iron solubility and speciated organics

Finally, the relationship between water-soluble iron and speciated organics, specifically naphthalene and IVOCs, was examined. In contrast with all other measured parameters, Fig. 4 shows relatively strong correlations between water-soluble iron and some of the IVOC species. Figure 4 presents the classifications which have the strongest correlation with water-soluble iron. Water-soluble iron relationships with other IVOCs can be found in the Supplement (Fig. S8). The correlation with water-soluble iron is highest for IVOC polar species with 16 carbons ($R^2 = 0.56$). The variance in Fig. 4 could result from the fact that, in addition to the IVOCs, other factors also influence iron water solubility.

As water-soluble iron trends well with naphthalene and polar IVOCs but not with bulk EC or OC, it is highly suggestive that iron solubility from the direct emission samples is primarily dependent on interactions with the species of carbon present in the particles during the extraction process. To better understand these interactions, a preliminary laboratory study was conducted to explore both (i) the effect of these organic compounds on iron solubility and (ii) the effect of soluble iron on the oxidation of organic compounds during the extraction process. Specifically, when naphthalene was added to an insoluble iron source (a soil), iron solubility increased from 0.8% to 4.2% of the total, or by a factor of ~ 5.5 , showing that the addition of naphthalene alone can

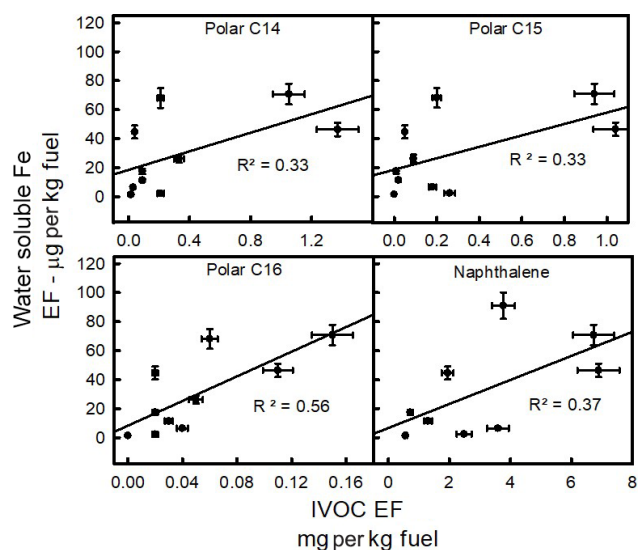


Figure 5. Scatter plots of water-soluble iron versus the sum of IVOCs reported in EF (grams per kilogram of fuel).

have a significant effect on iron water solubility and that this effect is likely important during the extraction process.

Lacking oxidized functional groups, naphthalene was not expected to chelate iron or to otherwise have the ability to increase iron solubility. Thus, we investigated what compounds are formed from naphthalene during these extractions. Figure 5 shows the new oxidized products formed from naphthalene during the water extraction. In the presence of soluble iron, HPLC retention time analysis shows the presence of phthalic acid (12.5 min), phthalic anhydride (7.5 min), and naphthol (15 min). The peaks at and below 5 min were not identified, but based on the retention times these are thought to be low-molecular-mass highly polar organic products and are consistent with other studies (Haynes et al., 2019).

3.4 Iron–carbon interactions

There are at least two methods in which organic compounds can lead to increased iron solubility: (a) reduction of Fe(III) to Fe(II) or (b) bringing soluble iron into solution via chelation. The first one is generally achieved by photochemistry (Pehkonen et al., 1993), which is not directly applicable to this study. The second, chelation, generally requires oxidized functional groups as shown in Fig. 5. The extent of the ability for phthalic acid (a dicarboxylic acid) to chelate iron has not been reported; however, it is known that similar-molecular-mass organic diacids have significant ability to chelate iron, thus pulling it into solution (Paris and Desboeufs, 2013). Here, we suggest that the observed correlations between IVOCs–naphthalene and water-soluble iron can be best explained with Fenton reactions, resulting in the propagation of radical reactions (Pehkonen et al., 1993). As shown from the Fe XANES valance plot, the iron is predominately Fe(III)

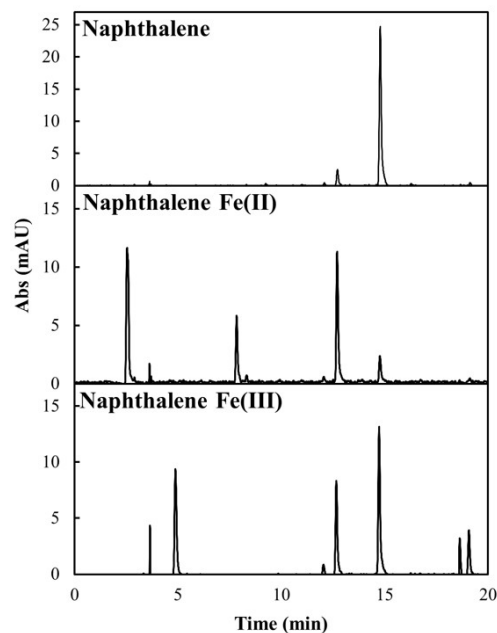
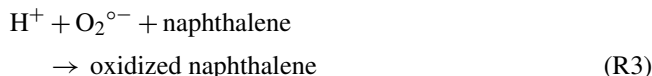
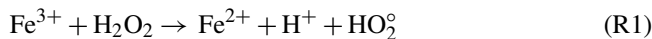


Figure 6. HPLC of resulting reaction between naphthalene and water-soluble iron. Phthalic acid at 12.5 min, phthalic anhydride at 7.5 min, naphthol at 15 min, and naphthalene at 20 min. The column uses a C18 stationary phase on beads with an 80 Å pore size.

(Fig. 4). In addition to the Fe(III), it has been shown that H_2O_2 forms in $\text{PM}_{2.5}$ water extracts, and it has been speculated that this formation is from various transition metals and/or quinones found in $\text{PM}_{2.5}$ (Wang et al., 2012).



In the presence of H_2O_2 , Fe(III) is known to undergo Reaction (1) (Neyens and Baeyens, 2003; Pignatello et al., 2006), resulting in the formation of Fe(II) and HO_2 (Pignatello et al., 2006; Rubio-Clemente et al., 2014), which degrades into superoxide, $\text{O}_2^{\circ-}$, and H^+ (Reaction 2). Superoxide has the ability to oxidize organic compounds, particularly aromatic structures (Reaction 3) (Lair et al., 2008). The resulting structures of these oxidized compounds typically have two oxygen atoms, which could be arranged in various functional groups (Lair et al., 2008; Rubio-Clemente et al., 2014) as observed from the HPLC chromatograms. Oxidized single-ring aromatic structures have a strong affinity to iron and have the ability chelate iron into aqueous solution (Haynes and Majestic, 2019; Hosseini and Madarshahian, 2009). Based on the laboratory studies of naphthalene and soluble iron presented here, naphthalene and/or IVOC oxidation during the extraction process is the most likely path towards increased iron solubility in primary tailpipe emissions. This overall process

suggests that Fe(III) is emitted through car exhaust; through interaction with water and organics it undergoes a Fenton-like reaction for conversion to Fe(II), and the iron is chelated by the resulting oxidized organics.

4 Conclusions

This study shows that water-soluble iron is directly formed from vehicle exhaust and not correlated with sulfates. The results show that iron is solubilized in water by specific organic compounds present in automobile exhaust and that soluble iron is not necessarily dictated by the overall OC content. Thus, the implication is that anthropogenic water-soluble iron is a result of chelation from specific organic compounds, likely their eventual aqueous reaction products. Although the mechanism of these aqueous transformations was not directly measured in this study, based on Fenton chemistry, the primary compounds are expected to be oxidized versions of naphthalene and/or IVOCs (Ledakowicz et al., 1999). Since these oxidation reactions occur fairly quickly (i.e., during the water extraction), further studies are of interest to better understand how these organic compounds interact with iron as it enters atmospheric waters and also the photochemical interactions between iron and organics.

Data availability. The data used in this study are available upon request from the corresponding author.

Supplement. The supplement related to this article is available online at: <https://doi.org/10.5194/acp-20-1849-2020-supplement>.

Author contributions. The sample collection scheme was designed by ALR, AHG, and BJM. Samples were collected by BTC and GTD. Organic speciation was performed by GTD. Trace elements were quantified by JRS. Iron speciation was performed by JRS, RYM, and BJM, with the interpretation effort led by SCF. Benchtop naphthalene experiments were performed by JPH. Data integration was performed by JRS. The paper was prepared by JRS and BJM.

Competing interests. The authors declare that they have no conflict of interest.

Acknowledgements. The authors thank the excellent and dedicated personnel at the California Air Resources Board, especially at the Haagen-Smit Laboratory. This study was funded by the National Science Foundation under grant numbers 1342599 and 1549166. This research used resources of the Advanced Light Source, which is a DOE Office of Science User Facility, under contract no. DE-AC02-05CH11231. Financial support was provided by the California Air Resources Board (contract no. 12-318). The California Air

Resources Board also provided substantial in-kind support for vehicle procurement, testing, and emissions characterization.

Financial support. This research has been supported by the US National Science Foundation (grant nos. 1342599 and 1549166) and the California Air Resources Board (grant no. 12-318).

Review statement. This paper was edited by Harald Saathoff and reviewed by two anonymous referees.

References

- Baba, Y., Yatagai, T., Harada, T., and Kawase, Y.: Hydroxyl radical generation in the photo-fenton process: Effects of carboxylic acids on iron redox cycling, *Chem. Eng. J.*, 277, 229–241, <https://doi.org/10.1016/j.cej.2015.04.103>, 2015.
- Baker, A. R., Jickells, T. D., Witt, M., and Linge, K. L.: Trends in the solubility of iron, aluminium, manganese and phosphorus in aerosol collected over the Atlantic Ocean, *Mar. Chem.*, 98, 43–58, <https://doi.org/10.1016/j.marchem.2005.06.004>, 2006.
- Bonnet, S.: Dissolution of atmospheric iron in seawater, *Geophys. Res. Lett.*, 31, L03303, <https://doi.org/10.1029/2003GL018423>, 2004.
- Cartledge, B. T. and Majestic, B. J.: Metal concentrations and soluble iron speciation, *Atmos. Pollut. Res.*, 6, 495–505, 2015.
- Cartledge, B. T., Marcotte, A. R., Herckes, P., Anbar, A. D., and Majestic, B. J.: The Impact of Particle Size, Relative Humidity, and Sulfur Dioxide on Iron Solubility in Simulated Atmospheric Marine Aerosols, *Environ. Sci. Technol.*, 49, 7179–7187, <https://doi.org/10.1021/acs.est.5b02452>, 2015.
- Chen, H. and Grassian, V. H.: Iron Dissolution of Dust Source Materials during Simulated Acidic Processing: The Effect of Sulfuric, Acetic, and Oxalic Acids, *Environ. Sci. Technol.*, 47, 10312–10321, <https://doi.org/10.1021/es401285s>, 2013.
- Chen, Y. and Siefert, R. L.: Seasonal and spatial distributions and dry deposition fluxes of atmospheric total and labile iron over the tropical and subtropical North Atlantic Ocean, *J. Geophys. Res.-Atmos.*, 109, D09305, <https://doi.org/10.1029/2003JD003958>, 2004.
- Cheung, K. L., Ntziachristos, L., Tzamkiozis, T., Schauer, J. J., Samaras, Z., Moore, K. F., and Sioutas, C.: Emissions of particulate trace elements, metals and organic species from gasoline, diesel, and biodiesel passenger vehicles and their relation to oxidative potential, *Aerosol Sci. Tech.*, 44, 500–513, <https://doi.org/10.1080/02786821003758294>, 2010.
- Chuang, P. Y., Duvall, R. M., Shafer, M. M., and Schauer, J. J.: The origin of water soluble particulate iron in the Asian atmospheric outflow, *Geophys. Res. Lett.*, 32, 1–4, <https://doi.org/10.1029/2004GL021946>, 2005.
- Desboeufs, K. V., Losno, R., Vimeux, F., and Cholbi, S.: The pH-dependent dissolution of wind-transported Saharan dust, *J. Geophys. Res.*, 104, 21287–21299, 1999.
- Drozd, G. T., Zhao, Y., Saliba, G., Frodin, B., Maddox, C., Weber, R. J., Chang, M. C. O., Maldonado, H., Sardar, S., Robinson, A. L., and Goldstein, A. H.: Time Resolved Measurements of Speciated Tailpipe Emissions from Motor Vehi-

- cles: Trends with Emission Control Technology, Cold Start Effects, and Speciation, *Environ. Sci. Technol.*, 50, 13592–13599, <https://doi.org/10.1021/acs.est.6b04513>, 2016.
- Drozd, G. T., Zhao, Y., Saliba, G., Frodie, B., Maddox, C., Chang, M.-C. O., Maldonado, H., Sardar, S., Weber, R. J., Robinson, A. L., and Goldstein, A. H.: Detailed Speciation of Intermediate Volatility and Semivolatile Organic Compound Emissions from Gasoline Vehicles: Effects of Cold-Starts and Implications for Secondary Organic Aerosol Formation, *Environ. Sci. Technol.*, 53, 1706–1714, 2019.
- Faiola, C., Johansen, A. M., Rybka, S., Nieber, A., Thomas, C., Bryner, S., Johnston, J., Engelhard, M., Nachimuthu, P., and Owens, K. S.: Ultrafine particulate ferrous iron and anthracene associations with mitochondrial dysfunction, *Aerosol Sci. Tech.*, 45, 1109–1122, <https://doi.org/10.1080/02786826.2011.581255>, 2011.
- Fu, H., Lin, J., Shang, G., Dong, W., Grassian, V. H., Carmichael, G. R., Li, Y., and Chen, J.: Solubility of Iron from Combustion Source Particles in Acidic Media Linked to Iron Speciation, *Environ. Sci. Technol.*, 46, 11119–11127, <https://doi.org/10.1021/es302558m>, 2012.
- Gao, Y.: Aeolian iron input to the ocean through precipitation scavenging: A modeling perspective and its implication for natural iron fertilization in the ocean, *J. Geophys. Res.*, 108, 4221, <https://doi.org/10.1029/2002JD002420>, 2003.
- Goldstein, A., Robinson, A., Kroll, J., Drozd, G., Zhao, Y., Saliba, G., Saleh, R., and Presto, A.: Investigating Semi-Volatile Organic Compound Emissions from Light-Duty Vehicles, California Air Resources Board, Contract No. 12-318, 225 pp., 2017.
- Hamad, S. H., Schauer, J. J., Antkiewicz, D. S., Shafer, M. M., and Kadhim, A. K. H.: ROS production and gene expression in alveolar macrophages exposed to PM_{2.5} from Baghdad, Iraq: Seasonal trends and impact of chemical composition, *Sci. Total Environ.*, 543, 739–745, <https://doi.org/10.1016/j.scitotenv.2015.11.065>, 2016.
- Hand, J. L., Mahowald, N. M., Chen, Y., Siefert, R. L., Luo, C., Subramaniam, A., and Fung, I.: Estimates of atmospheric-processed soluble iron from observations and a global mineral aerosol model: Biogeochemical implications, *J. Geophys. Res.-Atmos.*, 109, 1–21, <https://doi.org/10.1029/2004JD004574>, 2004.
- Haynes, J. and Majestic, B.: Role of polycyclic aromatic hydrocarbons on the photo-catalyzed solubilization of simulated soil-bound atmospheric iron, *Atmos. Pollut. Res.*, 11, 583–589, <https://doi.org/10.1016/j.apr.2019.12.007>, 2019.
- Haynes, J. P., Miller, K. E., and Majestic, B. J.: Investigation into Photoinduced Auto-Oxidation of Polycyclic Aromatic Hydrocarbons Resulting in Brown Carbon Production, *Environ. Sci. Technol.*, 53, 682–691, <https://doi.org/10.1021/acs.est.8b05704>, 2019.
- Hickox, W. H., Werner, B., and Gaffney, P.: Air Resources Board, (Mld), 1–6, available at: http://www.arb.ca.gov/ei/see/memo_ag_emission_factors.pdf (last access: 11 April 2018), 2000.
- Hosseini, M. S. and Madarshahian, S.: Investigation of charge transfer complex formation between Fe(III) and 2,6-Dihydroxy benzoic acid and its applications for spectrophotometric determination of iron in aqueous media, *E-J. Chem.*, 6, 985–992, <https://doi.org/10.1155/2009/417303>, 2009.
- Jickells, T. D., An, Z. S., Andersen, K. K., Baker, A. R., Bergametti, G., Brooks, N., Cao, J. J., Boyd, P. W., Duce, R. A., Hunter, K. A., Kawahata, H., Kubilay, N., LaRoche, J., Liss, P. S., Mahowald, N., Prospero, J. M., Ridgwell, A. J., Tegen, I., and Torres, R.: Global iron connections between desert dust, ocean biogeochemistry, and climate, *Science*, 308, 67–71, <https://doi.org/10.1126/science.1105959>, 2005.
- Kraemer, S. M.: Iron oxide dissolution and solubility in the presence of siderophores, *Aquat. Sci.*, 66, 3–18, <https://doi.org/10.1007/s00027-003-0690-5>, 2004.
- Kraft, S., Stümpel, J., and Becker, P.: High resolution x-ray absorption spectroscopy with absolute energy calibration for the determination of absorption edge energetics, *Rev. Sci. Instrum.*, 67, 681–687, <https://doi.org/10.1063/1.1146657>, 1996.
- Kuang, X. M., Scott, J. A., da Rocha, G. O., Betha, R., Price, D. J., Russell, L. M., Cocker, D. R., and Paulson, S. E.: Hydroxyl radical formation and soluble trace metal content in particulate matter from renewable diesel and ultra low sulfur diesel in at-sea operations of a research vessel, *Aerosol Sci. Tech.*, 51, 147–158, <https://doi.org/10.1080/02786826.2016.1271938>, 2017.
- Lair, A., Ferronato, C., Chovelon, J. M., and Herrmann, J. M.: Naphthalene degradation in water by heterogeneous photocatalysis: An investigation of the influence of inorganic anions, *J. Photoch. Photobio. A*, 193, 193–203, <https://doi.org/10.1016/j.jphotochem.2007.06.025>, 2008.
- Landreman, A. P., Shafer, M. M., Hemming, J. C., Hannigan, M. P., and Schauer, J. J.: A Macrophage-Based Method for the Assessment of the Reactive Oxygen Species (ROS) Activity of Atmospheric Particulate Matter (PM) and Application to Routine (Daily-24 h) Aerosol Monitoring Studies, *Aerosol Sci. Tech.*, 42, 946–957, <https://doi.org/10.1080/02786820802363819>, 2008.
- Lawrence, S., Sokhi, R., Ravindra, K., Mao, H., Prain, H. D., and Bull, I. D.: Source apportionment of traffic emissions of particulate matter using tunnel measurements, *Atmos. Environ.*, 77, 548–557, <https://doi.org/10.1016/j.atmosenv.2013.03.040>, 2013.
- Ledakowicz, S., Miller, J. S., and Olejnik, D.: Oxidation of PAHs in water solutions by ultraviolet radiation combined with hydrogen peroxide, *Int. J. Photoenergy*, 1, 1–6, <https://doi.org/10.1155/S1110662X99000100>, 1999.
- Lee, R. E. and Von Lehmden, D. J.: Trace metal pollution in the environment, *J. Air Pollut. Control Assoc.*, 23, 853–857, <https://doi.org/10.1080/00022470.1973.10469854>, 1973.
- Li, Y. and Xiang, R.: Particulate pollution in an underground car park in Wuhan, China, *Particuology*, 11, 94–98, <https://doi.org/10.1016/j.partic.2012.06.010>, 2013.
- Liati, A., Pandurangi, S. S., Boulouchos, K., Schreiber, D., and Arroyo Rojas Dasilva, Y.: Metal nanoparticles in diesel exhaust derived by in-cylinder melting of detached engine fragments, *Atmos. Environ.*, 101, 34–40, <https://doi.org/10.1016/j.atmosenv.2014.11.014>, 2015.
- Lough, G. C., Schauer, J. J., Park, J. S., Shafer, M. M., Deminter, J. T., and Weinstein, J. P.: Emissions of metals associated with motor vehicle roadways, *Environ. Sci. Technol.*, 39, 826–836, <https://doi.org/10.1021/es048715f>, 2005.
- Luo, C., Mahowald, N. M., Meskhidze, N., Chen, Y., Siefert, R. L., Baker, A. R., and Johansen, A. M.: Estimation of iron solubility from observations and a global aerosol model, *J. Geophys. Res.-Atmos.*, 110, 1–23, <https://doi.org/10.1029/2005JD006059>, 2005.
- Luo, C., Mahowald, N., Bond, T., Chuang, P. Y., Artaxo, P., Siefert, R., Chen, Y., and Schauer, J.: Combustion iron distri-

- bution and deposition, *Global Biogeochem. Cy.*, 22, GB1012, <https://doi.org/10.1029/2007GB002964>, 2008.
- Mackie, D. S., Boyd, P. W., Hunter, K. A., and McTainsh, G. H.: Simulating the cloud processing of iron in Australian dust: pH and dust concentration, *Geophys. Res. Lett.*, 32, 1–4, <https://doi.org/10.1029/2004GL022122>, 2005.
- Majestic, B. J., Schauer, J. J., and Shafer, M. M.: Application of synchrotron radiation for measurement of iron red-ox speciation in atmospherically processed aerosols, *Atmos. Chem. Phys.*, 7, 2475–2487, <https://doi.org/10.5194/acp-7-2475-2007>, 2007.
- Majestic, B. J., Anbar, A. D., and Herckes, P.: Elemental and iron isotopic composition of aerosols collected in a parking structure, *Sci. Total Environ.*, 407, 5104–5109, <https://doi.org/10.1016/j.scitotenv.2009.05.053>, 2009.
- Marcus, M. A., Macdowell, A. A., Celestre, R., Manceau, A., Miller, T., Padmore, H. A., and Sublett, R. E.: Beamline 10.3.2 at ALS: a hard X-ray microprobe for environmental and materials sciences, *J. Synchrotron Radiat.*, 11, 239–247, <https://doi.org/10.1107/S0909049504005837>, 2004.
- Marcus, M. A., Westphal, A. J., and Fakra, S. C.: Classification of Fe-bearing species from K-edge XANES data using two-parameter correlation plots, *J. Synchrotron Radiat.*, 15, 463–468, <https://doi.org/10.1107/S0909049508018293>, 2008.
- May, A. A., Nguyen, N. T., Presto, A. A., Gordon, T. D., Lipsky, E. M., Karve, M., Gutierrez, A., Robertson, W. H., Zhang, M., Brandow, C., Chang, O., Chen, S., Cicero-Fernandez, P., Dinkins, L., Fuentes, M., Huang, S. M., Ling, R., Long, J., Maddox, C., Massetti, J., McCauley, E., Miguel, A., Na, K., Ong, R., Pang, Y., Rieger, P., Sax, T., Truong, T., Vo, T., Chattopadhyay, S., Maldonado, H., Maricq, M. M., and Robinson, A. L.: Gas- and particle-phase primary emissions from in-use, on-road gasoline and diesel vehicles, *Atmos. Environ.*, 88, 247–260, <https://doi.org/10.1016/j.atmosenv.2014.01.046>, 2014.
- Moore, J. K. and Abbott, M. R.: Surface chlorophyll concentrations in relation to the Antarctic Polar Front: Seasonal and spatial patterns from satellite observations, *J. Mar. Syst.*, 37, 69–86, [https://doi.org/10.1016/S0924-7963\(02\)00196-3](https://doi.org/10.1016/S0924-7963(02)00196-3), 2002.
- Neyens, E. and Baeyens, J.: A review of classic Fenton's peroxidation as an advanced oxidation technique, *J. Hazard. Mater.*, 98, 33–50, [https://doi.org/10.1016/S0304-3894\(02\)00282-0](https://doi.org/10.1016/S0304-3894(02)00282-0), 2003.
- Norbeck, J. M., Durbin, T. D., and Truex, T. J.: Measurement of primary particulate matter emissions from light-duty motor vehicles, Coordinating Research Council, Inc. and South Coast Air Quality Management District, Riverside, CA, TS22, 1998.
- Oakes, M., Weber, R. J., Lai, B., Russell, A., and Ingall, E. D.: Characterization of iron speciation in urban and rural single particles using XANES spectroscopy and micro X-ray fluorescence measurements: investigating the relationship between speciation and fractional iron solubility, *Atmos. Chem. Phys.*, 12, 745–756, <https://doi.org/10.5194/acp-12-745-2012>, 2012a.
- Oakes, M., Ingall, E. D., Lai, B., Shafer, M. M., Hays, M. D., Liu, Z. G., Russell, A. G., and Weber, R. J.: Iron solubility related to particle sulfur content in source emission and ambient fine particles, *Environ. Sci. Technol.*, 46, 6637–6644, <https://doi.org/10.1021/es300701c>, 2012b.
- Paris, R. and Desboeufs, K. V.: Effect of atmospheric organic complexation on iron-bearing dust solubility, *Atmos. Chem. Phys.*, 13, 4895–4905, <https://doi.org/10.5194/acp-13-4895-2013>, 2013.
- Paris, R., Desboeufs, K. V., and Journet, E.: Variability of dust iron solubility in atmospheric waters: Investigation of the role of oxalate organic complexation, *Atmos. Environ.*, 45, 6510–6517, <https://doi.org/10.1016/j.atmosenv.2011.08.068>, 2011.
- Park, S., Nam, H., Chung, N., Park, J.-D., and Lim, Y.: The role of iron in reactive oxygen species generation from diesel exhaust particles, *Toxicol. Vitro.*, 20, 851–857, <https://doi.org/10.1016/j.tiv.2005.12.004>, 2006.
- Pehkonen, S. O., Siefert, R., Erel, Y., Webb, S., and Hoffmann, M. R.: Photoreduction of Iron Oxyhydroxides in the Presence of Important Atmospheric Organic Compounds, *Environ. Sci. Technol.*, 27, 2056–2062, <https://doi.org/10.1021/es00047a010>, 1993.
- Pignatello, J. J., Oliveros, E., and MacKay, A.: Advanced oxidation processes for organic contaminant destruction based on the Fenton reaction and related chemistry, *Crit. Rev. Env. Sci. Tec.*, 36, 1–84, <https://doi.org/10.1080/10643380500326564>, 2006.
- Rubio-Clemente, A., Torres-Palma, R. A., and Peñuela, G. A.: Removal of polycyclic aromatic hydrocarbons in aqueous environment by chemical treatments: A review, *Sci. Total Environ.*, 478, 201–225, <https://doi.org/10.1016/j.scitotenv.2013.12.126>, 2014.
- Saliba, G., Saleh, R., Zhao, Y., Presto, A. A., Lambe, A. T., Frodin, B., Sardar, S., Maldonado, H., Maddox, C., May, A. A., Drozd, G. T., Goldstein, A. H., Russell, L. M., Hagen, F., and Robinson, A. L.: Comparison of Gasoline Direct-Injection (GDI) and Port Fuel Injection (PFI) Vehicle Emissions: Emission Certification Standards, Cold-Start, Secondary Organic Aerosol Formation Potential, and Potential Climate Impacts, *Environ. Sci. Technol.*, 51, 6542–6552, <https://doi.org/10.1021/acs.est.6b06509>, 2017.
- Santos, D. S. S., Korn, M. G. A., Guida, M. A. B., Santos, G. L. dos, Lemos, V. A., and Teixeira, L. S. G.: Determination of copper, iron, lead and zinc in gasoline by sequential multi-element flame atomic absorption spectrometry after solid phase extraction, *J. Braz. Chem. Soc.*, 22, 552–557, 2011.
- Schauer, J. J., Kleeman, M. J., Cass, G. R., and Simoneit, B. R. T.: Measurement of emissions from air pollution sources. 5. C1–C32 organic compounds from gasoline-powered motor vehicles, *Environ. Sci. Technol.*, 36, 1169–1180, <https://doi.org/10.1021/es0108077>, 2002.
- Sedwick, P. N., Sholkovitz, E. R., and Church, T. M.: Impact of anthropogenic combustion emissions on the fractional solubility of aerosol iron: Evidence from the Sargasso Sea, *Geochem. Geophys. Geosy.*, 8, 10, <https://doi.org/10.1029/2007GC001586>, 2007.
- Shi, Z., Krom, M. D., Jickells, T. D., Bonneville, S., Carslaw, K. S., Mihalopoulos, N., Baker, A. R., and Benning, L. G.: Impacts on iron solubility in the mineral dust by processes in the source region and the atmosphere: A review, *Aeolian Res.*, 5, 21–42, <https://doi.org/10.1016/j.aeolia.2012.03.001>, 2012.
- Sholkovitz, E. R., Sedwick, P. N., and Church, T. M.: Influence of anthropogenic combustion emissions on the deposition of soluble aerosol iron to the ocean: Empirical estimates for island sites in the North Atlantic, *Geochim. Cosmochim. Ac.*, 73, 3981–4003, <https://doi.org/10.1016/j.gca.2009.04.029>, 2009.
- Sholkovitz, E. R., Sedwick, P. N., Church, T. M., Baker, A. R., and Powell, C. F.: Fractional solubility of aerosol iron: Synthesis of a global-scale data set, *Geochim. Cosmochim. Ac.*, 89, 173–189, <https://doi.org/10.1016/j.gca.2012.04.022>, 2012.

- Stumm, W. and Morgan, J. J.: Aquatic Chemistry: Chemical Equilibria and Rates in Natural Water, 3rd ed., Wiley-Interscience, 1996.
- Tagliabue, A., Bowie, A. R., Philip, W., Buck, K. N., Johnson, K. S., and Saito, M. A.: Review The integral role of iron in ocean biogeochemistry, *Nat. Publ. Gr.*, 543, 51–59, <https://doi.org/10.1038/nature21058>, 2017.
- Teixeira, L. S. G., Rocha, R. B. S., Sobrinho, E. V., Guimarães, P. R. B., Pontes, L. A. M., and Teixeira, J. S. R.: Simultaneous determination of copper and iron in automotive gasoline by X-ray fluorescence after pre-concentration on cellulose paper, *Talanta*, 72, 1073–1076, <https://doi.org/10.1016/j.talanta.2006.12.042>, 2007.
- Verma, V., Fang, T., Guo, H., King, L., Bates, J. T., Peltier, R. E., Edgerton, E., Russell, A. G., and Weber, R. J.: Reactive oxygen species associated with water-soluble PM_{2.5} in the southeastern United States: spatiotemporal trends and source apportionment, *Atmos. Chem. Phys.*, 14, 12915–12930, <https://doi.org/10.5194/acp-14-12915-2014>, 2014.
- Vile, G. F., Winterbourn, C. C., and Sutton, H. C.: Radical-driven fenton reactions: Studies with paraquat, adriamycin, and anthraquinone 6-sulfonate and citrate, ATP, ADP, and pyrophosphate iron chelates, *Arch. Biochem. Biophys.*, 259, 616–626, [https://doi.org/10.1016/0003-9861\(87\)90528-5](https://doi.org/10.1016/0003-9861(87)90528-5), 1987.
- Wang, Y., Arellanes, C., and Paulson, S. E.: Hydrogen peroxide associated with ambient fine-mode, diesel, and biodiesel aerosol particles in Southern California, *Aerosol Sci. Tech.*, 46, 394–402, <https://doi.org/10.1080/02786826.2011.633582>, 2012.
- Zhao, Y., Nguyen, N. T., Presto, A. A., Hennigan, C. J., May, A. A., and Robinson, A. L.: Intermediate Volatility Organic Compound Emissions from On-Road Diesel Vehicles: Chemical Composition, Emission Factors, and Estimated Secondary Organic Aerosol Production, *Environ. Sci. Technol.*, 49, 11516–11526, <https://doi.org/10.1021/acs.est.5b02841>, 2015.
- Zhao, Y., Nguyen, N. T., Presto, A. A., Hennigan, C. J., May, A. A., and Robinson, A. L.: Intermediate Volatility Organic Compound Emissions from On-Road Gasoline Vehicles and Small Off-Road Gasoline Engines, *Environ. Sci. Technol.*, 50, 4554–4563, <https://doi.org/10.1021/acs.est.5b06247>, 2016.
- Zhu, X., Prospero, J. M., Savoie, D. L., Millero, F. J., Zika, R. G., and Saltzman, E. S.: Photoreduction of iron(III) in marine mineral aerosol solutions, *J. Geophys. Res.-Atmos.*, 98, 9039–9046, <https://doi.org/10.1029/93JD00202>, 1993.